Förster resonance energy transfer, absorption and emission spectra in multichromophoric systems. III. Exact stochastic path integral evaluation

Jeremy M. Moix, Jian Ma, and Jianshu Cao

Citation: The Journal of Chemical Physics **142**, 094108 (2015); doi: 10.1063/1.4908601
View online: http://dx.doi.org/10.1063/1.4908601
View Table of Contents: http://scitation.aip.org/content/aip/journal/jcp/142/9?ver=pdfcov
Published by the AIP Publishing

Förster resonance energy transfer, absorption and emission spectra in multichromophoric systems. III. Exact stochastic path integral evaluation

Jeremy M. Moix, Jian Ma, and Jianshu Cao[a)]
Department of Chemistry, Massachusetts Institute of Technology, 77 Massachusetts Avenue, Cambridge, Massachusetts 02139, USA

(Received 13 August 2014; accepted 6 February 2015; published online 3 March 2015)

A numerically exact path integral treatment of the absorption and emission spectra of open quantum systems is presented that requires only the straightforward solution of a stochastic differential equation. The approach converges rapidly enabling the calculation of spectra of large excitonic systems across the complete range of system parameters and for arbitrary bath spectral densities. With the numerically exact absorption and emission operators, one can also immediately compute energy transfer rates using the multi-chromophoric Förster resonant energy transfer formalism. Benchmark calculations on the emission spectra of two level systems are presented demonstrating the efficacy of the stochastic approach. This is followed by calculations of the energy transfer rates between two weakly coupled dimer systems as a function of temperature and system-bath coupling strength. It is shown that the recently developed hybrid cumulant expansion (see Paper II) is the only perturbative method capable of generating uniformly reliable energy transfer rates and emission spectra across a broad range of system parameters. © *2015 AIP Publishing LLC.* [http://dx.doi.org/10.1063/1.4908601]

I. INTRODUCTION

The far-field absorption and emission spectra are standard experimental tools in the characterization of excitonic systems. The temperature and solvent dependence of these spectra are often used to extract a wealth of information on, for example, the microscopic geometry of the constituent chromophores, the coupling strength between the excitonic system and its environment, as well as the relative importance of heterogeneous broadening mechanisms.[1–3] Despite this wide applicability, at present there are still relatively few theoretical approaches that are capable of providing uniformly reliable estimates of the spectra of open quantum systems. Only in the limiting case that the spectrum arises from a single isolated electronic transition can the exact absorption and emission spectra be obtained analytically (up to a numerical integration) through cumulant expansion techniques.[4] However, in the more common setting, wherein the excitonic complexes are comprised of multiple coupled chromophores, then one must, in general, resort to numerical methods. Unfortunately, there is no numerically exact approach currently available for systems containing more than a few chromophores that are valid over a large range of the parameter space. As a result, comparisons between many interesting experimental systems and their corresponding microscopic theoretical models are often out of reach. One of the central aims of this work is to fill this gap. Here, we present an efficient path integral approach that allows one to compute the numerically exact absorption and emission spectra of multi-chromophoric open quantum systems.

Due to the lack of robust exact methods, one often turns to perturbative techniques. As detailed in the preceding papers of this series (henceforth referred to as Papers I[5] and II[6]), many of the standard approximate approaches are capable of generating reliable absorption spectra, as only the short time dynamics of a factorized system-environment initial state are required. The emission spectrum, however, presents a much more challenging problem. In this case, the real-time dynamics evolve from the correlated equilibrium state of the entire excitonic system and its environment. Unless the system-bath coupling is very weak, perturbative treatments often generate qualitatively incorrect emission spectra and generally become even worse as the temperature is lowered.[5,7] One of the major results of the previous papers in this series was a hybrid perturbative method capable of providing reliable emission spectrum over a broad range of system parameters.[6] The approach is not fully perturbative in that it combines the knowledge of the numerically exact equilibrium reduced density matrix, which can be obtained relatively easily through imaginary time path integral methods,[8] with an approximate cumulant expansion of the remaining real time dynamics. This initial state correction becomes essential at low temperatures or strong coupling. The hybrid cumulant expansion (HCE) thus greatly extends the parameter regimes accessible to perturbative methods and generally improves the quality of the results.

In the context of numerically exact treatments of the emission spectrum, such as the hierarchy equation of motion (HEOM),[9] the problem of a correlated system-bath initial state is overcome by simply preparing a factorized state sufficiently far in the past such that the system has reached equilibrium at time zero. As a result, these approaches

a)jianshu@mit.edu

require an initial lengthy propagation of the reduced density matrix to equilibrium before the dynamics of the dipole correlation function can be calculated.[10,11] Furthermore, as these approaches rely on efficient representations of the influence functional, they are generally restricted to environments that are not strongly non-Markovian. The main result of this paper is a stochastic path integral approach that circumvents many of the restrictions imposed by other numerically exact methods and, in particular, is applicable for arbitrary spectral densities and temperatures.

While an exact calculation of the absorption and emission spectra is important in its own right, it also provides an additional benefit. That is, one can immediately compute energy transfer rates between weakly coupled excitonic systems using the multi-chromophoric Förster resonant energy transfer (MCFT) formalism. The MCFT framework is a generalization of the standard Förster theory to the situation where the donor or acceptor complex consists of multiple coupled chromophores[12] and has gained recent attention as this scenario appears to be one of most common motifs employed in the highly efficient energy transfer networks found in biological systems. For example, the light harvesting systems found in both green and purple bacteria are comprised of independent complexes of strongly coupled chromophores that form the base units for large-scale energy transfer networks.[14,15]

In Sec. II, the details of the MCFT formalism are presented. There, it becomes apparent that the key quantities necessary for computing energy transfer rates are generalized operators related to the absorption spectrum of the acceptor complex and the emission spectrum of the donor. Then, we present the path integral treatment of the absorption operator and demonstrate that it may be efficiently computed as the solution to a straightforward stochastic differential equation. This approach is then generalized to the emission spectrum by taking advantage of the detailed balance condition that relates the emission operator to its corresponding absorption operator evolving in a complex time. Following these formal developments, numerical calculations are presented for model two level systems that can be reliably benchmarked against the HEOM approach. The temperature dependence of the emission spectrum is presented, followed by systematic calculations of the MCFT rate as a function of the temperature and system-bath coupling strength. It is observed that the hybrid cumulant expansion technique developed in Paper II is the only perturbative approach that provides uniformly reliable results for the energy transfer rates.[6] In a forthcoming work, the path integral and HCE methods will be used to provide the first systematic analysis of the energy transfer rates between two B850 complexes in the light harvesting system LH2.[16]

II. MCFT FORMALISM

The MCFT formalism has been expounded in the previous papers in this series. Here, we provide only the salient details necessary to keep the presentation self-contained. The total system is composed of a donor complex consisting of $N_{\rm D}$ chromophores that are weakly coupled to an acceptor complex of $N_{\rm A}$ chromophores. The Hamiltonian for the entire donor-acceptor system is then

$$H = H^{\rm D} + H^{\rm A} + H^{\rm DA}, \tag{1}$$

where $H^{\rm D(A)}$ denotes the Hamiltonian operator of the multi-chromophoric donor (acceptor) complex along with its associated thermal environment. The excitonic coupling between the donor and acceptor systems is characterized by $H^{\rm DA}$, which, within the local basis of the single-excitation subspace of the donor and acceptor, is given by

$$H^{\rm DA} = \sum_{n=1}^{N_{\rm D}} \sum_{m=1}^{N_{\rm A}} J^{\rm DA}_{nm} \left|D_n\right\rangle \left\langle A_m\right| . \tag{2}$$

The Hamiltonian of an individual complex is modeled as a general open quantum system,

$$H^{\alpha} = H^{\alpha}_{\rm s} + H^{\alpha}_{\rm b} + H^{\alpha}_{\rm sb}, \tag{3}$$

where the label $\alpha \in (D, A)$ serves to distinguish between the donor and acceptor systems. The free excitonic Hamiltonian of each complex is given by

$$H^{\alpha}_{\rm s} = \sum_{m=1}^{N_\alpha} (\epsilon^{\alpha}_m + \lambda^{\alpha}_m) \left|\alpha_m\right\rangle \left\langle \alpha_m\right| + \sum_{n\neq m}^{N_\alpha} t^{\alpha}_{nm} \left|\alpha_n\right\rangle \left\langle \alpha_m\right| , \tag{4}$$

where ϵ_m is the excitation energy of the mth chromophore, t_{nm} denotes the intra-complex electronic couplings, and λ_m is the environment-induced reorganization energy. The free bath Hamiltonian is

$$H^{\alpha}_{\rm b} = \sum_{m=1}^{N_\alpha} \sum_{k} \hbar\omega^{\alpha}_{m,k} b^{\alpha\dagger}_{m,k} b^{\alpha}_{m,k}, \tag{5}$$

where $b^{\alpha\dagger}_{m,k}$ ($b^{\alpha}_{m,k}$) denotes the respective creation (annihilation) operator of the kth mode of the bath with frequency $\omega^{\alpha}_{m,k}$ and coupled to chromophore m on the excitonic complex labeled by α. The system bath coupling is linear in the bath coordinates, and assumed to modulate only the excitation energies,

$$H^{\alpha}_{\rm sb} = \sum_{m=1}^{N_\alpha} V^{\alpha}_m \sum_{k} g^{\alpha}_{m,k} \left(b^{\alpha\dagger}_{m,k} + b^{\alpha}_{m,k}\right), \tag{6}$$

where $V^{\alpha}_m = \left|\alpha_m\right\rangle \left\langle \alpha_m\right|$ and $g^{\alpha}_{m,k}$ denotes the coupling strength.

Assuming that the exciton lifetime is much longer than the timescale associated with the energy transfer, then relaxation to the ground state can be safely ignored, and the population transfer rate between the donor and acceptor systems is given by the MCFT rate formula

$$k = 2{\rm Re} \int_0^{\infty} dt\ {\rm Tr}\left[\left(H^{\rm DA}\right)^{\top} \mathbf{E}^{\rm D}(t) H^{\rm DA} \mathbf{I}^{\rm A}(t)\right], \tag{7}$$

which can be easily obtained from the golden rule expression as shown in Sec. II of Paper I.[5] The absorption operator of the acceptor, $\mathbf{I}^{\rm A}(t)$, and emission operator of the donor, $\mathbf{E}^{\rm D}(t)$, appearing in Eq. (7) are formally defined as

$$\mathbf{I}^{\rm A}(t) = {\rm Tr}_{\rm b}\left[e^{-\frac{i}{\hbar}H^{\rm A}t} \rho^{\rm A} e^{+\frac{i}{\hbar}H^{\rm A}_{\rm b}t}\right], \tag{8}$$

$$\mathbf{E}^{\rm D}(t) = {\rm Tr}_{\rm b}\left[e^{+\frac{i}{\hbar}H^{\rm D}t} \rho^{\rm D} e^{-\frac{i}{\hbar}H^{\rm D}_{\rm b}t}\right]. \tag{9}$$

In the case of the absorption operator, the initial density matrix corresponds to a factorized state of the system

and bath, $\rho^{\mathrm{A}} = I_{\mathrm{s}} \otimes e^{-\beta H_{\mathrm{b}}^{\mathrm{A}}}/Z_{\mathrm{b}}^{\mathrm{A}}$, due to the assumption of a Franck-Condon transition from the ground state. The steady-state emission, however, occurs after the total system has equilibrated within the single excitation manifold. Thus, the initial state in Eq. (9) corresponds to the equilibrium state of the entire system and bath, $\rho^{\mathrm{D}} = e^{-\beta H^{\mathrm{D}}}/Z^{\mathrm{D}}$, where $Z^{\mathrm{D}} = \mathrm{Tr}\left[e^{-\beta H^{\mathrm{D}}}\right]$ is the partition function of the donor. As discussed extensively in the previous papers of the series, the difference in the initial states is the key feature that distinguishes the absorption from the emission operator, with the correlated initial condition in Eq. (9) leading to a substantially more involved calculation.

A. Detailed balance

The absorption and emission spectra obey a well-known detailed balance condition, and it is readily apparent that their corresponding operators in Eqs. (8) and (9) must obey a similar relation. In the frequency domain, the detailed balance condition for the operators reads

$$\mathbf{E}^{\mathrm{D}}(\omega) = \frac{e^{\hbar\beta\omega}}{Z}\mathbf{I}^{\mathrm{D}}(\omega), \tag{10}$$

where $Z = Z^{\mathrm{D}}/Z_{\mathrm{b}}^{\mathrm{D}}$. Thus, in principle, knowledge of the absorption operator allows for a straightforward determination of the corresponding emission operator. However, in practice, the thermal prefactor exponentially amplifies any error in the absorption data leading to an ill-conditioned numerical problem. As a result, Eq. (10) is generally of little practical use outside of the very high temperature limit.

An alternative approach can be based on the observation that in the time domain, the detailed-balance condition takes the form

$$\mathbf{E}^{\mathrm{D}}(t)^{*} = \frac{1}{Z}\mathbf{I}^{\mathrm{D}}(t - i\hbar\beta), \tag{11}$$

where the asterisk denotes complex conjugation. That is, through the straightforward substitution, $t \to t - i\hbar\beta$, the time evolution of the emission operator of the donor is equivalent to that of the absorption operator, except that the dynamics evolves in complex time rather than in purely real time. In contrast to the frequency-domain detailed balance relation, the time-domain version in Eq. (11) is free from numerical instabilities and forms the basis for the developments presented here. Here, we employ the path integral formalism to develop an exact and efficient numerical treatment of the spectral operators rather than pursue perturbative approaches as were explored in the previous papers of this series. In Subsection II B, the stochastic path integral representation for the absorption operator is presented and then generalized to the case of emission through the rotation from real time to complex time suggested by Eq. (11).

B. Absorption operator

As can be seen from Eq. (8), the absorption operator does not require the full time evolution of the reduced density matrix. The bath evolves both forward and backward in time, but the system is only propagated forward in time. As a result, we can still take advantage of the influence functional formalism from the path integral approach to open quantum systems,[17] but we only need a single path for the system variables. Thus, the absorption operator can be determined from the path integral expression

$$U^{\mathrm{A}}(t) = \int \mathcal{D}[\sigma] e^{\frac{i}{\hbar}S_0^{\mathrm{A}}[\sigma]} F[\sigma], \tag{12}$$

where $S_0^{\mathrm{A}}[\sigma]$ denotes the action associated with the free system Hamiltonian of the acceptor, $H_{\mathrm{s}}^{\mathrm{A}}$, and the standard boundary conditions of the paths have been suppressed for clarity. The Feynman-Vernon influence functional, $F[\sigma]$, obtained by integrating out each of the N_{A} independent baths is given by

$$F[\sigma] = \prod_{n=1}^{N_{\mathrm{A}}} \exp\left(-\frac{1}{\hbar}\int_0^t dt' \int_0^{t'} dt'' V_n^{\mathrm{A}}(\sigma(t')) \times V_n^{\mathrm{A}}(\sigma(t''))C_n(t'-t'')\right). \tag{13}$$

All of the microscopic details of the baths that are relevant to the system dynamics enter through their respective correlation functions in the influence functional, which take the standard form

$$C_n(t) = \frac{1}{\pi}\int_0^{\infty} d\omega\ J_n(\omega) \times \left[\coth(\hbar\beta\omega/2)\cos(\omega t) - i\sin(\omega t)\right], \tag{14}$$

with the spectral density function

$$J_n(\omega) = \frac{\pi}{2}\sum_k \frac{g_{n,k}^2}{\omega_{n,k}}\delta(\omega - \omega_{n,k}). \tag{15}$$

One of the great benefits of the path integral formalism is that it places no restrictions upon the functional form of the spectral density as opposed to many other approaches to open quantum systems.

Following our previous developments on the equilibrium reduced density matrix,[8] as well as those of several others on the full real time dynamics of the density matrix,[18,19] the nonlocality present in the influence functional can be substituted for local interactions with stochastic auxiliary fields, which can then be efficiently sampled through Monte Carlo methods. Formally, this is affected by applying a separate Hubbard-Stratonovich transformation to each of the N_{A} terms in the influence functional. Then, Eq. (13) can be exactly rewritten as

$$F[\sigma] = \prod_{n=1}^{N_{\mathrm{A}}} \int \mathcal{D}[\xi_n]\ w_n \exp\left(-\frac{1}{2\hbar}\int_0^t dt' \int_0^t dt'' \xi_n(t') \times C_n^{-1}(t'-t'')\xi_n(t'') + \frac{i}{\hbar}\int_0^t dt' V_n^{\mathrm{A}}(\sigma(t'))\xi_n(t')\right), \tag{16}$$

where w_n represents the normalization constant of the Gaussian functional integral associated with the nth bath. The path integral involving the system variables is now completely local in time and the auxiliary fields can be reinterpreted as a source of colored noise driving the system dynamics. Thus, individual samples of the absorption operator can be simply

and straightforwardly calculated through the solution of a stochastic differential equation,

$$\frac{d}{dt}\rho^{\mathrm{A}}(t) = -\frac{i}{\hbar}H^{\mathrm{A}}(t)\rho^{\mathrm{A}}(t), \tag{17}$$

subject to the initial condition $\rho^{\mathrm{A}}(0) = I_{\mathrm{s}}$. The stochastic Hamiltonian is given by

$$H^{\mathrm{A}}(t) = H_{\mathrm{s}}^{\mathrm{A}} + \sum_n \xi_n(t) V_n^{\mathrm{A}}, \tag{18}$$

and the *scalar*, complex-valued, Gaussian noise terms obey the correlations

$$\begin{aligned} \langle \xi_n(t) \rangle &= 0, \\ \langle \xi_n(t)\xi_m(t') \rangle &= \delta_{nm} C_n(t-t')/\hbar. \end{aligned} \tag{19}$$

The exact time evolution of the absorption operator is obtained after averaging the stochastic dynamics over realizations of the noise, $\mathbf{I}^{\mathrm{A}}(t) = \langle \rho^{\mathrm{A}}(t) \rangle_{\xi}$. Here, we have assumed that each of the baths is independent of all others. To include correlated baths, one need only to replace the delta function in Eq. (19) with the desired spatial correlations. The generation of complex, Gaussian colored noise is discussed in Appendix A.

The stochastic path integral equation for the absorption operator bears some similarity to the non-Markovian quantum state diffusion (NMQSD) approach recently proposed to compute the zero temperature absorption spectrum of excitonic systems.[20] While NMQSD is formally exact, all practical implementations to date have relied on approximations. In contrast, the present Eq. (17) is both formally and numerically exact, although it may prove fruitful to further explore the connections between the two approaches.

C. Emission operator

Due to the correlated initial state, the calculation of the emission operator is considerably more involved than that of the absorption. The propagator in the path integral representation is[17]

$$U^{\mathrm{D}}(t,\hbar\beta) = \int \mathcal{D}[\sigma] \int \mathcal{D}[\bar{\sigma}] e^{-\frac{i}{\hbar}S_0^{\mathrm{D}}[\sigma] - \frac{1}{\hbar}S_0^{E,\mathrm{D}}[\bar{\sigma}]} F[\sigma,\bar{\sigma}], \tag{20}$$

where $S_0^{E,D}$ denotes the Euclidean action of the donor system Hamiltonian associated with the initial imaginary time propagation to the equilibrium state. The influence functional now contains three contributions from the respective propagations in real time, imaginary time, and the correlations between the two,

$$\begin{aligned} F[\sigma,\bar{\sigma}] = \prod_n^{N_D} &\exp\left(-\frac{1}{\hbar}\int_0^t dt' \int_0^{t'} dt''\, V_n^{\mathrm{D}}(\sigma(t')) V_n^{\mathrm{D}}(\sigma(t'')) C_n(t'-t'') \right) \\ &\times \exp\left(\frac{1}{\hbar}\int_0^{\hbar\beta} d\tau' \int_0^{\tau'} d\tau''\, V_n^{\mathrm{D}}(\bar{\sigma}(\tau')) V_n^{\mathrm{D}}(\bar{\sigma}(\tau'')) C_n(-i\tau' + i\tau'') \right) \\ &\times \exp\left(\frac{i}{\hbar}\int_0^{\hbar\beta} d\tau' \int_0^{t} dt'\, V_n^{\mathrm{D}}(\bar{\sigma}(\tau')) V_n^{\mathrm{D}}(\sigma(t')) C_n^*(t'-i\tau') \right). \end{aligned} \tag{21}$$

The bath correlation function is defined for complex arguments through the analytic continuation of Eq. (14) as[17]

$$C_n(z) = \frac{1}{\pi}\int_0^{\infty} d\omega J_n(\omega) \frac{\cosh(\hbar\beta\omega/2 - i\omega z)}{\sinh(\hbar\beta\omega/2)}, \tag{22}$$

where $z = t - i\tau$ and $0 \le \tau \le \hbar\beta$.

As is readily seen, the path integral expression for the emission operator is considerably more complicated than the corresponding result for the absorption operator. Additionally, the coupling between the real and imaginary time paths in the influence functional prevents a straightforward application of the Hubbard-Stratonovich transformation as was used previously for the absorption operator. Fortunately, a simplification is possible. The detailed balance relation in Eq. (11) suggests that the emission operator may be computed in an identical manner to the absorption through the introduction of a complex time variable $z = t - i\hbar\beta$. Indeed, with this substitution in the path integral expressions above, the emission propagator may then be defined in an analogous fashion to Eq. (12) except along a time-ordered contour in the complex time plane,[17]

$$U^{\mathrm{D}}(z) = \int \mathcal{D}[\sigma] e^{-\frac{i}{\hbar}S_0^{\mathrm{D}}[\sigma]} F[\sigma]. \tag{23}$$

The influence functional similarly simplifies to

$$\begin{aligned} F[\sigma] = \prod_n^{N_D} \exp\Bigg(-\frac{1}{\hbar}\int_0^z dz' \int_{z'>z''} dz''\, V_n^{\mathrm{D}}(\sigma(z')) \\ \times V_n^{\mathrm{D}}(\sigma(z'')) C_n(z'-z'') \Bigg). \end{aligned} \tag{24}$$

With these results, the Hubbard-Stratonovich transformations and stochastic Schrödinger equation are then formally equivalent to those of the absorption operator presented in Sec. II B. The complex time evolution of samples of the emission operator obeys the equation

$$\frac{d}{dz}\rho^{\mathrm{D}}(z) = -\frac{i}{\hbar}H^{\mathrm{D}}(z)\rho^{\mathrm{D}}(z), \tag{25}$$

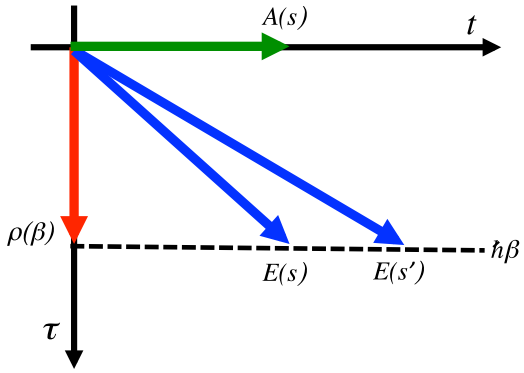

FIG. 1. The integration contours in the complex time plane $z = t - i\tau$ used in the various calculations. Integrating along $z = t$ (green arrow) yields the absorption operator while the contour $z = -i\tau$ (red arrow) results in the equilibrium reduced matrix. The blue arrows characterize the independent contours needed to generate the emission operator at times s and s'.

where the integration proceeds from time $z = 0$ to the complex time $z = t - i\hbar\beta$ subject to the initial condition, $\rho^{\mathrm{D}}(0) = I_s$. Similarly, the stochastic complex time-dependent Hamiltonian is given by

$$H^{\mathrm{D}}(z) = H_s^{\mathrm{D}} + \sum_n \xi_n(z) V_n^{\mathrm{D}}, \tag{26}$$

where the scalar noise components are again of zero mean and correlation,

$$\begin{aligned} \langle \xi_n(z) \rangle &= 0, \\ \langle \xi_n(z) \xi_m(z) \rangle &= \delta_{nm} C_n(z - z')/\hbar. \end{aligned} \tag{27}$$

As with the absorption, the numerically exact emission operator is obtained after the stochastic average over the noise variables, $\mathbf{E}^{\mathrm{D}}(t)^* = \langle \rho^{\mathrm{D}}(t - i\hbar\beta) \rangle_\xi / \langle Z \rangle_\xi$, where $Z = \mathrm{Tr}\left[\rho^{\mathrm{D}}(-i\hbar\beta)\right]$.

It should be noted that the stochastic path integral expression in Eq. (25) represents a generalized form of the stochastic propagation. It contains two interesting limits that are represented schematically in Fig. 1. For example, if the imaginary time component of the propagation is set to zero such that $z = t$, then one immediately recovers the absorption operator obtained above in Eq. (17). Alternatively, if the real time component of the integration contour is set to zero, then one recovers the pure imaginary time evolution of the equilibrium reduced density matrix propagation explored in our earlier work.[8] This leads to the interesting result that the emission operator at $t = 0$ is simply the exact equilibrium reduced density matrix.

D. Computational considerations

There are several points with regards to the stochastic formulation that should be emphasized. First, a generalized stochastic approach to compute the real time dynamics of the entire reduced density matrix has recently been explored.[18,19,21] In that case, the presence of complex noise generally leads to very slow convergence of the stochastic average as the length of the simulation increases. The approach presented here, and, in particular, Eq. (17), represents a simplified version of those works and thus directly inherits their numerical difficulties. However, the redeeming feature of the present approach is that the decay time of the absorption and emission correlation functions is much shorter than the corresponding relaxation time of the pure real time dynamics. As a result, brute force convergence of the stochastic path integral is generally possible with a reasonable number of Monte Carlo samples ($10^5 - 10^6$), although the low temperature regime can be more demanding.

Second, there is a subtle difficulty that should be discussed with regards to the calculation of the emission spectrum. As seen from Fig. 1, the propagations to times $s - i\hbar\beta$ and $s' - i\hbar\beta$ evolve along different contours in the complex time plane. The bath correlation functions evaluated along these two contours are different, and thus the emission operators $\mathbf{E}(s)$ and $\mathbf{E}(s')$ require completely independent calculations. In principle, this should increase the cost of computing the emission spectrum by a factor of the number of time steps with respect to that of the absorption. However, this is not the case since the presence of the imaginary time component in the propagation greatly improves the convergence properties of the Monte Carlo calculation.[21,22] While the computational cost of the emission spectrum is more expensive, it is not prohibitive.

Finally, the inclusion of static disorder in the absorption operator calculation is trivial, but less so for that of the emission operator. In the former case, the averages over the noise and disorder commute, and thus the two may be computed simultaneously. That is, the disorder-averaged absorption spectrum should incur practically no additional computational cost over that of the bare absorption spectrum. However, the presence of the partition function in the denominator of the emission operator demands that the average over the disorder must be computed independently of the average over the noise. As a result, the disorder-averaged emission spectrum, although straightforward, may be quite costly from a computational perspective.

III. NUMERICAL RESULTS

Although the path integral formalism is valid for any spectral density, below we will focus on the standard Drude-Lorentz form so that benchmark results from the HEOM formalism can be obtained. In a forthcoming work, we will examine the influence of the spectral density on the spectra and energy transfer rates of the light harvesting system LH2.[16] The Drude spectrum is defined by

$$J(\omega) = 2\lambda \frac{\omega\gamma}{\omega^2 + \gamma^2}, \tag{28}$$

where γ is the cutoff frequency and the reorganization energy λ is defined such that

$$\lambda = \frac{1}{\pi} \int_0^\infty d\omega \, \frac{J(\omega)}{\omega}. \tag{29}$$

As is commonly assumed, we take the spectral densities for each of the independent baths to be equivalent and, unless otherwise specified, fix the reorganization energy at $\lambda = 200\ \mathrm{cm}^{-1}$ and the cutoff frequency to $\gamma = 53\ \mathrm{cm}^{-1}$ ($10\ \mathrm{ps}^{-1}$).

A. Emission spectra

Before presenting the MCFT rates, we will first focus on the far-field spectra. The absorption and emission spectra can be computed by combining the knowledge of the corresponding operators defined above in Eqs. (8) and (9) with the respective transition dipole moment vectors of the chromophores ($\vec{\mu}$) by

$$I_i^{\mathrm{A}}(\omega) = \int_{-\infty}^{\infty} dt\; e^{+i\omega t} \sum_{n,m} \left(\vec{\varepsilon}_i \cdot \vec{\mu}_m^{\mathrm{A}}\right)\left(\vec{\varepsilon}_i \cdot \vec{\mu}_n^{\mathrm{A}}\right) \mathbf{I}_{mn}^{\mathrm{A}}(t), \tag{30}$$

$$E_i^{\mathrm{D}}(\omega) = \int_{-\infty}^{\infty} dt\; e^{-i\omega t} \sum_{n,m} \left(\vec{\varepsilon}_i \cdot \vec{\mu}_m^{\mathrm{D}}\right)\left(\vec{\varepsilon}_i \cdot \vec{\mu}_n^{\mathrm{D}}\right) \mathbf{E}_{mn}^{\mathrm{D}}(t), \tag{31}$$

where $\vec{\varepsilon}_i$ is a unit vector characterizing the polarization of the incident radiation field that projects onto the dipole moment vector of each chromophore. As noted above, the path integral evaluation of the emission spectrum contains the absorption spectrum as a limiting case, and hence we will focus only on the former here.

As a preliminary benchmark calculation to prove the efficacy of the path integral approach, Fig. 2 displays the stochastic path integral results for the emission spectrum in the unbiased two level system that was explored in Papers I and II. The system Hamiltonian $H_{\mathrm{s}} = V\sigma_x$ with $V = 200\ \mathrm{cm}^{-1}$ leads to highly delocalized exciton states and thus serves as an interesting test case to assess the validity of the MCFT formalism as well as that of approximate perturbative approaches. For simplicity, the dipole moment operators have been chosen to be equivalent for each site and in each direction such that $\vec{\mu}_m = 1$ in Eqs. (30) and (31). Because of this choice, the spectra are determined from the simple sum of all of the elements of the emission operator (cf. Eq. (31)). In Fig. 2, the path integral results at 200 and 300 K are compared with the corresponding results from the standard HEOM approach shown with increasing number of Matsubara terms. The HEOM results are seen to eventually converge to the path integral results, although even for this relatively simple two level system, the hierarchy results are difficult to converge and require both a large number of hierarchy tiers as well as several Matsubara terms. At the lowest temperature of $T = 100$ K shown in Fig. 2, the standard hierarchy calculations cannot be converged with respect to the number of Matsubara terms, and the sHEOM approach must be used to generate the numerically exact results.[23,24] Note that at each temperature, the hierarchy results and present path integral results are in precise agreement. However, compared with the hierarchy calculations, the stochastic approach developed here is more straightforward both in terms of implementation and convergence. Additionally, since the stochastic formalism is a Monte Carlo method, it is trivially parallelized and free from the memory demands that plague other density matrix approaches such as the HEOM or QUAPI. In the case that further improvements to the computational efficiency of the emission path integral are necessary, a very useful and accurate approximation can be employed which is discussed in Appendix B.

As is readily seen, the spectra in Fig. 2(a) are comprised of two peaks centered around the eigenstates of the total system Hamiltonian. While the intensity of the peak at positive frequencies is nearly independent of temperature, that of the low energy peak steadily decreases and vanishes at the lowest temperature shown of $T = 100$ K. This is in stark contrast to the behavior expected from an isolated two level system where the emission spectrum can be computed analytically as

$$E(\omega) = \sum_{i=1}^{2} P_i \left(1 + \frac{V}{\epsilon_i}\right) \delta(\omega - \epsilon_i), \tag{32}$$

with the eigenstate energies, $\epsilon_{1,2} = \pm\sqrt{V^2 + \Delta^2}$, V is the electronic coupling, Δ is the bias, and the eigenstate population, $P_i = e^{-\beta\epsilon_i}/Z$. As seen from Eq. (32), the spectra are composed of two peaks centered at the eigenfrequencies of the system with intensities that are weighted by the respective Boltzmann populations of the two states. At low temperature, the population localizes in the ground state, and the spectrum shifts to the red. In Fig. 2, the opposite occurs and a blue shift is clearly seen with decreasing temperature. This behavior is a result of the strong system bath coupling. To demonstrate this effect more clearly, Fig. 2(b) displays the reorganization energy dependence of the emission spectra at the lowest

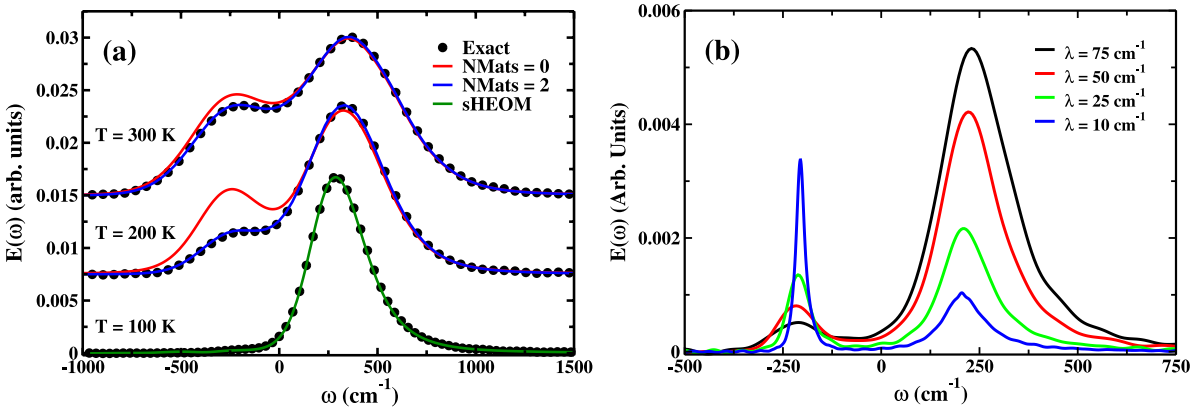

FIG. 2. (a) The emission spectrum at $T = 100$, 200, and 300 K in a model two level system comparing the present stochastic path integral calculations with the corresponding HEOM results with 0 (red) and 2 (blue) Matsubara terms. The number of hierarchy tiers required for convergence in each case is 12. The bath is defined by the reorganization energy $\lambda = 200\ \mathrm{cm}^{-1}$ and cutoff frequency $\gamma = 53\ \mathrm{cm}^{-1}$. For clarity, the results at $T = 200$ and 300 K are vertically offset by 0.0075 and 0.015, respectively. At $T = 100$ K, we cannot converge the standard HEOM and only the stochastic HEOM (green) formalism can produce reliable results. (b) The reorganization energy dependence of the emission spectrum at $T = 100$ K. The remaining parameters are the same as in (a).

temperature shown in Fig. 2(a) of $T = 100$ K. Only at very weak coupling, does the spectra resemble that expected for the isolated system from Eq. (32), with the emission dominated by the low energy eigenstate of the system. However, as the coupling increases in Fig. 2(b), the weighting of the two peaks is redistributed towards the higher lying eigenstate resulting in a steady shift to the blue. As discussed in Papers I and II, the equilibrium state of the total system and bath cannot be written in a factorized form as in Eq. (32), particularly when the temperature is low and the system-bath coupling large, as is the case here. This is the key feature that is responsible for the drastic failure of standard perturbative approximations to the emission spectra as well as the counterintuitive temperature dependence seen in Fig. 2(a).

B. MCFT rates

We next consider the multi-chromophoric energy transfer, where both the donor and acceptor complexes are comprised of the symmetric two level system analyzed in Fig. 2. That is, each complex is described by the system Hamiltonian, $H_s = V\sigma_x$, and the donor-acceptor couplings (Eq. (2)) are set to the constant value, $J_{nm}^{DA} = 10$ cm^{-1}. This weak coupling ensures that the perturbative MCFT formalism is valid and is also characteristic of many natural systems.[5] The energy transfer rates computed as a function of the system-bath coupling strength are displayed in Fig. 3(a). Although not shown, the rates from the HEOM formalism are in precise agreement with the present path integral results in the region where the former can be converged (up to $\lambda = 600$ cm^{-1}). As the transfer occurs between two symmetric systems, the transfer rates are monotonically decreasing functions of the system-bath coupling strength as would be expected from a simple analysis based on the standard Förster theory.

Also included in Fig. 3(a) is a comparison of the exact energy transfer rates with many of the commonly used perturbative methods. The TC2 is the standard second order, time-convolution master equation previously explored.[13] As it is based upon the approximation of weak system-bath coupling, its validity is rather limited and is generally inapplicable to many interesting physical systems, such as light-harvesting complexes, where the system-environment couplings cannot be considered as small. The full cumulant expansion (FCE) explored in Paper I and Ref. 7 provides reliable results over a much larger region of the parameter space as compared with the TC2, although it too begins to break down at very large system-bath couplings and eventually produces unphysical negative rates. The failure of both the TC2 and the FCE lies in their inaccurate treatment of the correlated initial state. Clearly, a perturbative expansion around a factorized initial state is qualitatively incorrect at large-system bath coupling. In order to overcome this difficulty, Paper II explored an expansion around the numerically exact equilibrium reduced density matrix, which can be straightforwardly obtained through imaginary time path integral techniques.[8] As seen in Fig. 3(a), this HCE technique provides a uniformly reliable approximation to the energy transfer rate, even at very strong system bath couplings.

Fig. 3(b) displays the temperature dependence of the MCFT rates. Qualitatively, the results follow the predictions of Marcus theory displaying a maximum as a function of temperature. However, the Marcus rate formula predicts a maximum at $2\lambda/k_B \approx 600$ K which is considerably lower than that observed from the exact calculations. Additionally, Marcus theory predicts that the energy transfer rate should vanish as the temperature decreases to zero. This is clearly not borne out in the exact results as the MCFT rates decrease to a finite value at low temperature due to non-vanishing quantum fluctuations. As with the system-bath coupling dependence, the approximate perturbative results are also included. It is seen that below room temperature, the accuracy of the FCE quickly degrades and eventually produces negative energy transfer rates. The results from the TC2 method are outside the scale of the graph at all temperatures, which is not entirely unexpected as the system-bath coupling strength here is of comparable magnitude to all the other system parameters. However, the hybrid method provides reliable results across the entire parameter range and also captures the plateau in the rates at low temperature. In a forthcoming work, it is demonstrated that the HCE is capable of capturing the temperature and system-bath coupling dependence of the energy transfer rates between two LH2 complexes while

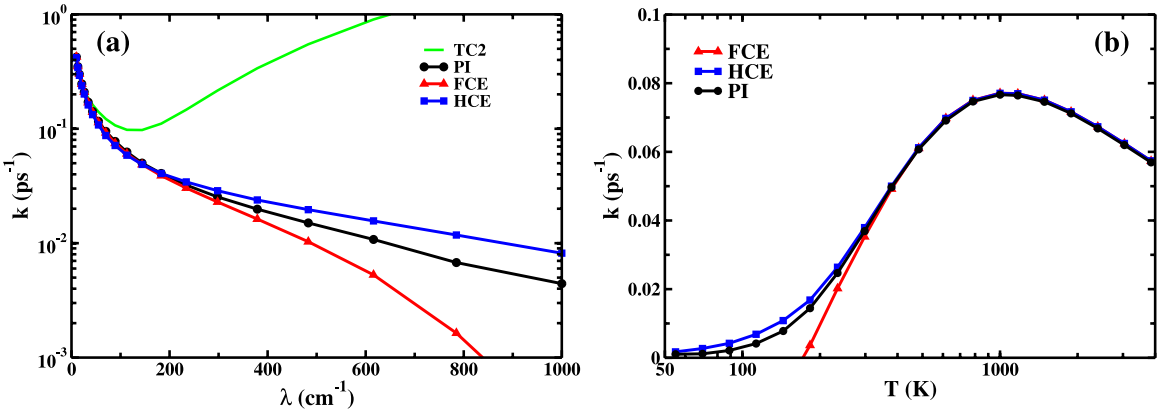

FIG. 3. (a) Energy transfer rates between two symmetric two level systems as a function of the reorganization energy. The cutoff frequency is $\gamma = 53$ cm^{-1} and the temperature is $T = 300$ K. The black dots, green lines, red triangles, and blue squares denote the results from the present stochastic path integral approach, the TC2 master equation,[13] the FCE,[5,7] and the HCE,[6] respectively. (b) The energy transfer rates as a function of the temperature. The reorganization energy is $\lambda = 200$ cm^{-1} and the cutoff frequency is $\gamma = 53$ cm^{-1}. The results from the TC2 approach lie outside the scale of the graph for all temperatures shown.

the failure of the TC2 and FCE is even more dramatic than seen here.[16]

IV. CONCLUSIONS

A stochastic path integral approach to compute the energy transfer rates between weakly coupled multi-chromophoric complexes has been presented. As a consequence of the MCFT formalism, one also has immediate access to the exact steady-state far-field absorption and emission spectra of the respective donor and acceptor complexes. The calculations of the absorption and emission operators require only the straightforward numerical solution of a stochastic differential equation, and the only difficulty lies in the convergence of the Monte Carlo average. As opposed to many other numerically exact approaches, the method developed here is amenable to any form of the spectral density and can readily treat the low temperature and strong coupling regimes. To our knowledge, the present path integral approach is the only method currently available that can accommodate such a broad range of system parameters in relatively large excitonic systems.

The numerical results presented here provide a systematic analysis of the role of the temperature and system-bath coupling strength on the emission spectra and energy transfer rates in model multi-chromophoric systems. As seen in Fig. 3, the exact MCFT rates serve as a stringent benchmark for approximate analytic methods. Whereas the standard perturbative approaches often yield qualitatively incorrect results, the HCE technique developed in Paper II[6] can provide uniformly reliable results for the energy transfer rates across a large range of the physically accessible parameter space.

Note added in proof. Computer codes for stochastic simulations of absorption spectra, emission spectra, and Forster rates are available for download at http://web.mit.edu/jianshucaogroup/resources.html.

ACKNOWLEDGMENTS

This work was supported by the NSF (Grant No. CHE-1112825). J. Moix and J. Ma have been supported by the Center for Excitonics, an Energy Frontier Research Center funded by the US Department of Energy, Office of Science, Office of Basic Energy Sciences under Award No. DE-SC0001088. This work used the Extreme Science and Engineering Discovery Environment (XSEDE), which is supported by National Science Foundation Grant No. OCI-1053575.

APPENDIX A: NOISE SAMPLING

Sampling the complex noise required for the absorption and emission operators is not completely trivial. The main difficulty is that the bath correlation function must be reproduced by $\langle \xi(t)\xi(t')\rangle$ rather than the Hermitian form $\langle \xi^*(t)\xi(t')\rangle$. To proceed, the correlation function can be split into its real and imaginary components,

$$C(t) = C_r(t) + iC_i(t), \tag{A1}$$

and the influence functional rewritten as

$$F[\sigma] = \exp\left[-\frac{1}{2\hbar}\int_0^t dt' \int_0^t dt'' V(\sigma(t'))V(\sigma(t'')) \times [C_r(t'-t'') + iC_i(|t'-t''|)]\right]. \tag{A2}$$

Hubbard-Stratonovich transformations are then applied to each term separately, leading to

$$F[\sigma] = \int \mathcal{D}[\zeta]\, w_\zeta \exp\left[-\frac{1}{2\hbar}\int_0^t dt' \int_0^t dt'' \zeta(t')C_r^{-1}(t'-t'')\zeta(t'') + \frac{i}{\hbar}\int_0^t dt' V(\sigma(t'))\zeta(t')\right] \times \int \mathcal{D}[\nu]\, w_\nu \exp\left[-\frac{1}{2\hbar}\int_0^t dt' \int_0^t dt'' \nu(t')C_i^{-1}(|t'-t''|)\nu(t'') + \frac{1-i}{\sqrt{2}\hbar}\int_0^t dt' V(\sigma(t'))\nu(t')\right], \tag{A3}$$

where w_ζ and w_ν denote the respective normalization constants. Thus, the noise characteristics are

$$\begin{aligned} \langle \zeta(t)\rangle &= 0, & \langle \nu(t)\rangle &= 0, \\ \langle \zeta(t)\zeta(t')\rangle &= C_r(t-t'), & \langle \nu(t)\nu(t')\rangle &= C_i(|t-t'|), \end{aligned} \tag{A4}$$

and the autocorrelation function of the combined process, $\xi(t) = \zeta(t) + \sqrt{i}\nu(t)$, is readily seen to reproduce the desired bath correlation function, $C(t)$.

Numerically sampling the real noise governed by the correlation, $C_r(t)$, is straightforward since this kernel is strictly positive semi-definite. Sampling such noise has been discussed in detail in our previous works.[8,23] One simply filters white noise with a kernel computed from the Cholesky decomposition of the Toeplitz matrix constructed from $C_r(t)$.

Sampling the noise for the imaginary part of the correlation function is less straightforward. The kernel, $C_i(t)$, is not positive definite since $C_i(0) = 0$, so that the Cholesky decomposition approach is not applicable. To cope with this, we have employed the approach suggested in Refs. 21 and 25. First, an eigen decomposition of the correlation matrix, $C_{i,nm} = C_i(|t_n - t_m|)$, is performed, and the diagonal eigenvalue matrix is sorted into a non-negative ($\mathbf{\Lambda}^+$) matrix and the remainder ($\mathbf{\Lambda}^-$), which are both of the same dimension as $\mathbf{C}_i$, such that

$$\mathbf{C}_i = \mathbf{U}\left[\mathbf{\Lambda}^+ + \mathbf{\Lambda}^-\right]\mathbf{U}^T. \tag{A5}$$

The positive components are sampled in the usual fashion by filtering the appropriate kernel with white noise, while the negative components are sampled by taking the absolute value

of the negative eigenvalues followed by a rotation with the complex unit. The desired noise sequence is then given by

$$\vec{\nu} = \mathbf{U}^T \left[\left(\mathbf{\Lambda}^+\right)^{1/2} + i|\mathbf{\Lambda}^-|^{1/2} \right] \vec{\Omega}, \tag{A6}$$

where $\vec{\Omega}$ represents a realization of independent white noise terms. Using the properties of white noise, it is readily seen that the autocorrelation of $\nu(t)$ faithfully reproduces the desired imaginary part of the bath correlation function.

APPENDIX B: APPROXIMATE EMISSION

A very accurate approximation to the emission operator can be made by simply ignoring the imaginary part of the bath correlation function in Eq. (22). This simplification generally reduces the number of Monte Carlo samples required to converge the stochastic path integral by at least an order of magnitude. For the purely real-time dynamics of the absorption operator, ignoring $C_i(t)$ leads to an extended Haken-Strobl model which rarely provides satisfactory results. However, for the emission operator, the real-time and imaginary-time dynamics are intertwined so that the analysis is more subtle. In this case, there are still non-unitary contributions to the dynamics even if the Hamiltonian is purely real due to the complex-time evolution. To better understand this seemingly drastic approximation, it is useful to analyze the complex-time bath correlation function. It is readily seen that the bath correlation function evaluated along the imaginary time axis to $z = -i\hbar\beta$ is a purely real quantity for *any* spectral density. This case corresponds to the equilibrium reduced density matrix which is a purely real quantity if the Hamiltonian is real. Thus for small real times, during which time the emission operator has often substantially decayed, the imaginary part of the correlation function is also negligibly small. This approximation is particularly accurate in the high temperature limit where the increasingly broad emission spectra are a result of the increasingly rapid decay of the emission operator. In summary, in the short-time limit, ignoring $C_i(z)$ is a reasonable approximation. In Fig. 4, the exact results for the emission spectrum of the two level system are reproduced from Fig. 2 along with the corresponding results from the approximation scheme discussed here where the imaginary part of the complex-time bath correlation function has been set to zero. Only at the lowest temperature of $T = 100$ K are there any significant differences between the exact and approximate emission spectra. In fact, comparison with Fig. 2 indicates that even at $T = 300$ K, the approximate emission spectrum is more accurate than the HEOM results computed without including Matsubara terms.

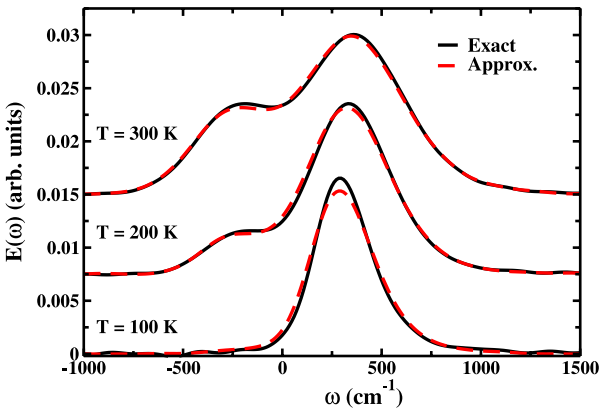

FIG. 4. The exact two-level system emission spectra reproduced from Fig. 2 (solid black) compared with the approximate emission spectra (dashed red) computed by ignoring the imaginary part of the bath correlation function. The parameters are identical to those in Fig. 2.

[1]D. Beljonne, C. Curutchet, G. D. Scholes, and R. J. Silbey, J. Phys. Chem. B **113**, 6583 (2009).
[2]D. J. Heijs, V. A. Malyshev, and J. Knoester, Phys. Rev. Lett. **95**, 177402 (2005).
[3]T. Renger, V. May, and O. Kühn, Phys. Rep. **343**, 137 (2001).
[4]S. Mukamel, *Principles of Nonlinear Optical Spectroscopy* (Oxford University Press, USA, 1999).
[5]J. Ma and J. Cao, "Förster resonance energy transfer, absorption and emission spectra in multichromophoric systems. I. Full cumulant expansions and system-bath entanglement," J. Chem. Phys. **142**, 094106 (2015).
[6]J. Ma, J. Moix, and J. Cao, "Förster resonance energy transfer, absorption and emission spectra in multichromophoric systems. II. Hybrid cumulant expansion," J. Chem. Phys. **142**, 094107 (2015).
[7]L. Banchi, G. Costagliola, A. Ishizaki, and P. Giorda, J. Chem. Phys. **138**, 184107 (2013).
[8]J. M. Moix, Y. Zhao, and J. Cao, Phys. Rev. B **85**, 115412 (2012).
[9]Y. Tanimura, J. Phys. Soc. Jpn. **75**, 082001 (2006).
[10]R. Xu and Y. Yan, Phys. Rev. E **75**, 031107 (2007).
[11]Y. Jing, L. Chen, S. Bai, and Q. Shi, J. Chem. Phys. **138**, 045101 (2013).
[12]H. Sumi, J. Phys. Chem. B **103**, 252 (1999).
[13]S. Jang, M. D. Newton, and R. J. Silbey, Phys. Rev. Lett. **92**, 218301 (2004).
[14]M. K. Sener, J. D. Olsen, C. N. Hunter, and K. Schulten, Proc. Natl. Acad. Sci. U. S. A. **104**, 15723 (2007).
[15]J. M. Olson, Photosynth. Res. **80**, 181 (2004).
[16]J. Moix, J. Ma, and J. Cao, "Exact evaluation of the energy transfer rates and steady state absorption and emission spectra in the b850 photosynthetic complexes of LH2" (unpublished).
[17]H. Grabert, P. Schramm, and G. Ingold, Phys. Rep. **168**, 115 (1988).
[18]J. T. Stockburger and H. Grabert, Phys. Rev. Lett. **88**, 170407 (2002).
[19]Y. Zhou, Y. Yan, and J. Shao, Europhys. Lett. **72**, 334 (2005).
[20]J. Roden, W. T. Strunz, and A. Eisfeld, J. Chem. Phys. **134**, 034902 (2011).
[21]J. Cao, L. W. Ungar, and G. A. Voth, J. Chem. Phys. **104**, 4189 (1996).
[22]B. J. Berne and D. Thirumalai, Annu. Rev. Phys. Chem. **37**, 401 (1986).
[23]J. M. Moix and J. Cao, J. Chem. Phys. **139**, 134106 (2013).
[24]L. Zhu, H. Liu, and Q. Shi, New J. Phys. **15**, 095020 (2013).
[25]Y. Zhou and J. Shao, J. Chem. Phys. **128**, 034106 (2008).